Guided Control of Human Drivers: Control Design and Experiments

Bence Szaksz, Gábor Orosz, *Senior Member, IEEE*, and Gabor Stepan

***Abstract*—This brief investigates the guidance of a human driver via an automated lead vehicle, when the automated vehicle is not only responding to a reference velocity but it also takes into account the speed of the subsequent human-driven vehicle (HV). To verify the theoretical results, a human-in-the-loop (HITL) simulation environment is developed, in which a graphical interface illustrates the automated vehicle ahead, while the human operator controls the velocity of the following vehicle via the accelerator and brake pedals. Nine human drivers were involved in the experiments, each of them carried out the driving task for 79 control gain combinations of the automated vehicle. Based on the measurement data, the parameters of the human driver model were estimated using the sweeping least squares method; the measurement results confirmed the applicability of the theoretical model in designing advanced traffic control strategies.**

***Index Terms*—Autonomous vehicles (AVs), human and vehicle interaction, human driving behavior, sweeping least squares method.**

I. Introduction

OVER the past few years, there has been significant progress in the development of automated driver assistant systems (ADAS) and autonomous vehicles (AVs). Despite these improvements, traditional human-driven vehicles (HVs) are still expected to maintain their dominance in traffic for a while yielding mixed traffic flows of AVs and HVs. Nevertheless, the integration of AVs into the traffic allows to mitigate accident risks [1], [2], [3], [4] and contribute to energy efficiency [5], [6], [7], thereby improving not only the AV's own performance but also benefiting the nearby traveling HVs [8].

Although, adaptive cruise control (ACC) offers valuable assistance to drivers, several studies presented that its overall impact on global traffic dynamics is limited [9], [10], [11]. This limitation arises from the constraint that each ACC-equipped vehicle responds only to its immediate predecessor. In contrast, AVs have the potential to gather information from connected vehicles that may be located further away in the traffic (and may be either human-driven or automated). This leads to the so-called connected cruise control (CCC) [2], [12], [13], [14] and connected traffic control (CTC) concepts [8], [15], [16], [17] depending on whether the connected vehicles are ahead or behind the connected automated vehicle (CAV), respectively. Finally, the vehicle to infrastructure communication should also be mentioned [18], [19] when the vehicles share information with a variety of devices supporting the traffic along a highway.

The potential of automated vehicles can only be realized if the human driving behavior is explored together with testing how AV interacts with human drivers. A straightforward option is to carry out experiments with real AVs and HVs on the roads [13], [20], [21], while driving simulator-based experiments [22], [23] also have their own benefits; the latter option is often called as human-in-the-loop (HITL) experiments. Beside their obvious low-cost, HITL experiments allow the exploration of critical parameter configurations that lead to dangerous traffic situations; these critical parameter configurations could not be studied in experiments involving real cars. This flexibility presents the relevance of HITL experiments before carrying out experiments on the roads.

In the literature, until now, limited attention has been given to how human drivers respond to the behavior of AVs in mixed traffic situations. Our primary motivation is to improve traffic efficiency and safety by better integrating AVs into mixed traffic; this study focuses on the case when an AV is providing guidance to a human driver operating the vehicle behind. The main novelty of this work lies in the control design of AVs while utilizing an HITL environment. The HITL results validate the human driver models with reaction time delay, and provide a good basis for future advanced controller design. The research contributes to a deeper understanding of how AVs can facilitate safer and more efficient driving while guiding nearby human drivers.

In this brief, we investigate the car following scenario, when an AV is traveling in front of an HV. The AV is not only equipped with cruise control but it also responds to its relative velocity with respect to the following HV; this allows a smooth guidance of the human driver [24], [25], [26]. A simulation environment is developed to investigate the corresponding mixed traffic dynamics. The graphical interface displays the automated lead vehicle, while the velocity of the following vehicle is controlled by a human operator via the accelerator and brake pedals. Using various control gain combinations of the AV, nine subjects carried out experiments. Based on these, the driving behaviors of the human operators are estimated

Received 13 March 2025; accepted 5 May 2025. Date of publication 3 June 2025; date of current version 23 October 2025. This work was supported by Hungarian National Research, Development and Innovation Office under Grant NKFI-KKP-133846. The work of Gábor Orosz was supported in part by Hungarian Academy of Sciences within the Distinguished Guest Fellowship Program in 2022 and in part by the Fulbright Foundation during 2023–2024. Recommended by Associate Editor Y. Yildiz. *(Corresponding author: Bence Szaksz.)*

Bence Szaksz is with the Department of Applied Mechanics, Budapest University of Technology and Economics, 1111 Budapest, Hungary, and also with the MTA-BME Lendület "Momentum" Global Dynamics Research Group, 1111 Budapest, Hungary (e-mail: szaksz@mm.bme.hu).

Gábor Orosz is with the Department of Mechanical Engineering and the Department of Civil and Environmental Engineering, University of Michigan, Ann Arbor, MI 48109 USA (e-mail: orosz@umich.edu).

Gabor Stepan is with the Department of Applied Mechanics, Budapest University of Technology and Economics, 1111 Budapest, Hungary (e-mail: stepan@mm.bme.hu).

Digital Object Identifier 10.1109/TCST.2025.3571601

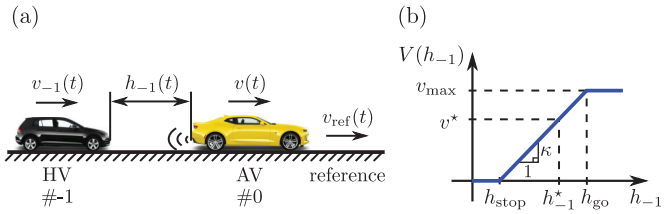

Fig. 1. (a) Schematic car following model. (b) Range policy function for the human driver model.

with the help of the sweeping least squares method [20], which allows the estimation of the human control gains and the relevant human reaction time simultaneously.

This brief is organized as follows. In Section II, the simplified car-following mathematical model is discussed, in which the dynamic behavior of the human operator is described with the optimal velocity model. Then, the developed HITL simulation environment is presented in Section III. The measurement results of the nine subjects are summarized in Section IV, which also contains the estimation of the parameters of the optimal velocity model. Finally, Section V presents the conclusions and discusses future research opportunities.

II. Modeling

Assume that an AV is traveling in front of an HV along a straight road. The velocity of the AV and that of the HV are denoted by v and v_{-1}, respectively, while the distance between the two vehicles is h_{-1} [see Fig. 1(a)]. A reference velocity v_{ref} is provided to the AV that also takes into account the velocity difference of the two vehicles. The optimal velocity model [2], [26], [27] is applied to approximate the behavior of the human driver, while this model will be replaced by a real human operator during the experiments. The corresponding governing equations take the form

$$\dot{h}_{-1}(t) = v(t) - v_{-1}(t) \tag{1}$$

$$\dot{v}_{-1}(t) = \alpha\left(V(h_{-1}(t-\tau)) - v_{-1}(t-\tau)\right) + \beta\left(W(v(t-\tau)) - v_{-1}(t-\tau)\right) \tag{2}$$

$$\dot{v}(t) = \hat{\beta}\left(v_{\text{ref}} - v(t-\sigma)\right) + \beta_{-1}\left(W(v_{-1}(t-\sigma)) - v(t-\sigma)\right) \tag{3}$$

where τ and σ denote the time delays at the HV and AV, respectively, while the control gains $\hat{\beta}$ and β_{-1} correspond to the cruise control gain and to the backward looking gain of the AV, respectively.

The human driver responds to the distance and the velocity difference between the two vehicles with the control gains α and β, respectively. The range policy function

$$V(h_{-1}) = \begin{cases} 0, & \text{if } h_{-1} < h_{\text{stop}} \\ F(h_{-1}), & \text{if } h_{-1} \in [h_{\text{stop}}, h_{\text{go}}] \\ v_{\max}, & \text{if } h_{-1} > h_{\text{go}} \end{cases} \tag{4}$$

describes the relationship between the distance headway h_{-1} and the corresponding desired velocity [see Fig. 1(b)]. If the headway gets smaller than the critical value h_{stop}, then the human driver aims to stop, while if the leading vehicle is at a sufficiently large distance $h > h_{\text{go}}$, then the driver intends to keep its reasonable maximal velocity $v_{\max}$. If the headway is within the interval $[h_{\text{stop}}, h_{\text{go}}]$, then the driver's response follows the monotonically increasing function $F(h_{-1})$. The simplest choice for the $F(h_{-1})$ function is to consider an affine function as it is visualized in Fig. 1(b). Furthermore, the speed policy $W(v) = \min\{v, v_{\max}\}$ is introduced to represent that the human driver does not want to follow the leader when that moves faster than $v_{\max}$. The same saturation function is used for the AV.

In the followings, let us consider that the possibly time-dependent reference velocity is a sum of the constant term $v^\star_{\text{ref}}$ and the small time dependent fluctuation $\tilde{v}_{\text{ref}}(t)$, that is, $v_{\text{ref}}(t) = v^\star_{\text{ref}} + \tilde{v}_{\text{ref}}(t)$. Then, assuming $\tilde{v}_{\text{ref}}(t) \equiv 0$, the steady-state solution of system (1) occurs when both vehicles travel with the same velocity $v^\star_{\text{ref}}$, while the steady-state headway is obtained from the corresponding inverse of the range policy function, that is, $h^\star_{-1} = V^{-1}(v^\star_{\text{ref}})$.

Let us introduce the state vector $\mathbf{x} = [\tilde{h}_{-1}\ \tilde{v}_{-1}\ \tilde{v}]^{\mathrm{T}}$ with

$$\tilde{h}_{-1} = h_{-1} - h^\star_{-1}, \quad \tilde{v}_{-1} = v_{-1} - v^\star_{\text{ref}}, \ \tilde{v} = v - v^\star_{\text{ref}}. \tag{5}$$

Both the reaction time of the human driver and the time delay required for the signal processing and actuation of the AV are relevant parameters to be considered. Taking these into account, the linearized dynamics at the steady state is governed by the delay differential equation (DDE)

$$\dot{\mathbf{x}}(t) = \mathbf{A}_0\mathbf{x}(t) + \mathbf{A}_\tau\mathbf{x}(t-\tau) + \mathbf{A}_\sigma\mathbf{x}(t-\sigma) + \mathbf{B}\tilde{v}_{\text{ref}} \tag{6}$$

with

$$\mathbf{A}_0 = \begin{bmatrix} 0 & -1 & 1 \\ 0 & 0 & 0 \\ 0 & 0 & 0 \end{bmatrix}, \quad \mathbf{A}_\tau = \begin{bmatrix} 0 & 0 & 0 \\ \alpha\kappa & -(\alpha+\beta) & \beta \\ 0 & 0 & 0 \end{bmatrix}$$
$$\mathbf{A}_\sigma = \begin{bmatrix} 0 & 0 & 0 \\ 0 & 0 & 0 \\ 0 & \beta_{-1} & -(\hat{\beta}+\beta_{-1}) \end{bmatrix}, \quad \mathbf{B} = \begin{bmatrix} 0 \\ 0 \\ \hat{\beta} \end{bmatrix}. \tag{7}$$

Here, κ is the slope of the range policy function at $h^\star_{-1}$.

The corresponding characteristic function takes the form

$$\begin{aligned} D(s) &:= \det\left(s\mathbf{I} - \mathbf{A}_0 - \mathbf{A}_\tau e^{-s\tau} - \mathbf{A}_\sigma e^{-s\sigma}\right) \\ &= s^3 + (\alpha+\beta)s^2e^{-s\tau} + (\hat{\beta}+\beta_{-1})s^2e^{-s\sigma} \\ &\quad + \left(\beta\hat{\beta} + \alpha\hat{\beta} + \alpha\beta_{-1}\right)se^{-s(\tau+\sigma)} + \alpha\kappa se^{-s\tau} \\ &\quad + \alpha\kappa\hat{\beta}e^{-s(\tau+\sigma)}. \end{aligned} \tag{8}$$

The linear system is exponentially stable if and only if all the infinitely many characteristic roots of the characteristic equation $D(s) = 0$ have negative real parts.

The stability boundaries in the plane of the control parameters of the AV are determined by means of the D-subdivision method [28, Ch. 2]. The static stability boundary (saddle-node (SN) boundary) is obtained by the substitution of $s = 0$ into the characteristic equation, yielding $\alpha\kappa\hat{\beta} = 0$. Assuming $\alpha > 0$ and $\kappa > 0$, this boundary is

$$\hat{\beta} = 0. \tag{9}$$

Furthermore, substituting $s = \mathrm{j}\Omega$ into the characteristic equation and separating the real and imaginary parts, one obtains the dynamic stability curves (Hopf curves) as a function of Ω

$$\beta_{-1}(\Omega) = \cos(\Omega\sigma)\frac{a(\Omega)}{c(\Omega)}, \quad \hat{\beta}(\Omega) = \frac{b(\Omega)}{c(\Omega)} \tag{10}$$

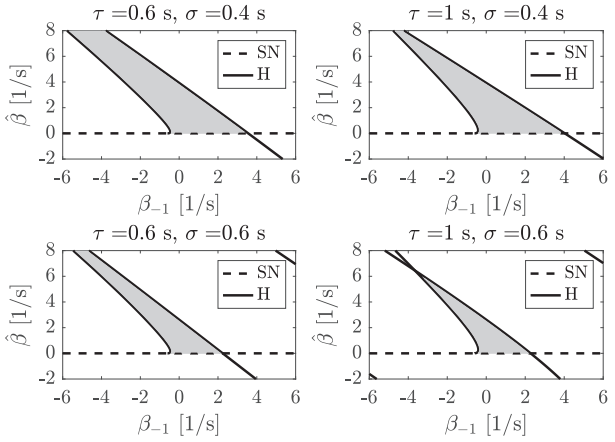

Fig. 2. Stability charts for different time delay combinations with HV parameters $\alpha = 0.25$ s^{-1}, $\beta = 0.3$ s^{-1}, and $\kappa = 0.6$ s^{-1}. The static SN and dynamic (Hopf, H) stability boundaries are shown by dashed and solid curves, respectively, and the stable domains are shaded.

where

$$a(\Omega) = -\Omega^4 + 2\Omega^3(\alpha+\beta)\sin(\Omega\tau) - \Omega^2\left((\alpha+\beta)^2 + 2\alpha\kappa\cos(\Omega\tau)\right) - \alpha^2\kappa^2 \quad (11)$$

$$b(\Omega) = \Omega^4\cos(\omega\sigma) + \Omega^2(\alpha^2+\alpha\beta)\cos(\Omega\sigma) - (\alpha+\beta)\Omega^3\sin(\Omega(\tau-\sigma)) - \alpha\Omega^3\sin(\Omega(\tau+\sigma)) - \alpha\kappa\Omega^2\cos(\Omega(\tau-\sigma)) + \alpha^2\kappa\Omega\sin(\Omega\sigma) \quad (12)$$

$$c(\Omega) = \beta\Omega^2\cos(\Omega\tau) - \alpha\kappa\Omega\sin(\Omega\tau) + \alpha^2\kappa. \quad (13)$$

Here, Ω refers to the angular frequency with which the system loses its stability when the parameters cross the dynamic stability boundary.

Fig. 2 presents stability charts in the plane of the control gains of the AV for various time delay combinations based on the closed form results (9)–(13). The dashed and the solid lines refer to the static (SN) and to the dynamic (Hopf) boundaries, respectively, while the stable regions are shaded. As it can be observed, the stable domain shrinks as the delays are increased, while it is more sensitive to the variation of the delay of the AV.

III. HITL Simulation Environment

The measurement setup consists of an Esperanza high-octane steering wheel and pedal [29], which is connected to the computer [Fig. 3(a)]. Note, that in this configuration, only the pedal signal is utilized, while the signal of the steering wheel is omitted. Still, the steering wheel is needed, since it forwards the pedal signal to the computer.

A HITL simulation environment was developed in MATLAB to verify the theoretical results. The human operator is sitting in front of a monitor, which displays the automated lead vehicle on a straight road such that the environment is projected to the vertical plane at the front bumper of the following vehicle. In order to have a real-time application with high enough sampling rate, the AV is inserted into the screen as a 2D image, the position and size of which is always adjusted to the actual distance between the vehicles.

Fig. 3(b) presents how the AV is projected for the human driver. We assume that the distance between the eye of the human operator and the front bumper of the HV is $d_0 = 2.5$ m, thus, the projected width of the AV is

$$w(t) = W\frac{d_0}{d_0 + h_{-1}(t)} \quad (14)$$

where W refers to the real width of the AV.

The projection of the $L_s = 4$ m long lane markers (of the center line) are similarly obtained, as shown in Fig. 3(c). Of course, the locations of these lane markers are updated according to the velocity of the HV. Let H and $d_s(t)$ denote the eye level of the driver and the distance between the front bumper and one of the lane markers, respectively. Then, the projection yields that the starting and the end points of the marker with respect to the horizon assume the form

$$H_{s,1}(t) = \frac{Hd_0}{d_0 + d_s(t)}, \quad H_{s,2}(t) = \frac{Hd_0}{d_0 + d_s(t) + L_s}, \quad (15)$$

respectively.

Fig. 3(d) presents the schematic model of the HITL simulation. Throughout the measurement process, the human operator manipulates the pedals based on the view of the graphical interface. The real-time application receives the signal of the pedals and adjusts the acceleration of the HV accordingly; it computes the response of the AV, and updates the graphical interface to reflect the state of the system in the subsequent timestep. This results in the time delay $\tau = \tau_h + \tau_c$ where τ_h and τ_c refer to the reaction delay of the human operator and to the computer delay, respectively.

The time integration is done based on the fourth-order Runge-Kutta method with the sampling time $\Delta t = 0.02$ s. The response of the AV is subject to an artificial delay $\sigma = 0.4$ s, while the maximum acceleration and deceleration of both vehicles are defined as $a_{\max} = 3$ m/s^2 and $a_{\min} = -7$ m/s^2, respectively. Note that the pedal is based on a potentiometer that provides the output signal with a resolution of 256 bits. Because of the inaccuracy of the potentiometer, this signal sometimes has 5%–10% error, but it can be tolerated since it does not influence the main results of the experiments.

The experiments started in a steady-state motion of the system, that is, the two vehicles traveled with the same velocity $v_{-1} = v = 10$ m/s in a distance of $h_{-1} = 15$ m, while the reference velocity was also set at $v_{\text{ref}} = 10$ m/s. Then a trapezoidal reference velocity profile was prescribed for the AV, which is visualized in Fig. 3(e). The AV followed the reference according to its control law (3), while the human operator was asked to drive as if it were a real traffic situation. To make the experiments more realistic, the brake lights of the AV were illuminated when it applied the brakes.

At first, we added a speedometer to the screen, which displayed the velocity of the HV. However, we realized that the operators quickly learned the prescribed velocity profile and then drove according to that and not according to the car-following situation. For the purpose of comparability of measurement results, we decided to use the same velocity profile, thus, finally, we omitted the speedometer that initiated the above mentioned (undesired) learning process. Instead, the speed of the lane markers shows the velocity of the HV, and a speed limit sign pops up if the corresponding velocity exceeds 25 m/s = 90 km/h.

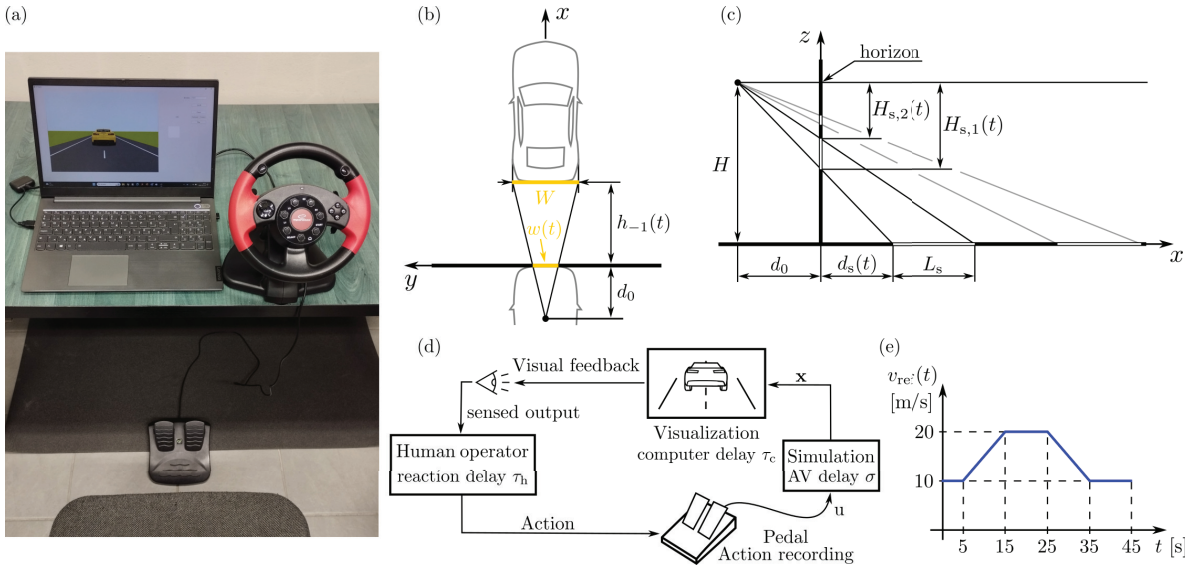

Fig. 3. (a) Measurement setup. (b) and (c) Projections of the environment. (d) Schematic of the HITL experiment. (e) Applied reference velocity profile.

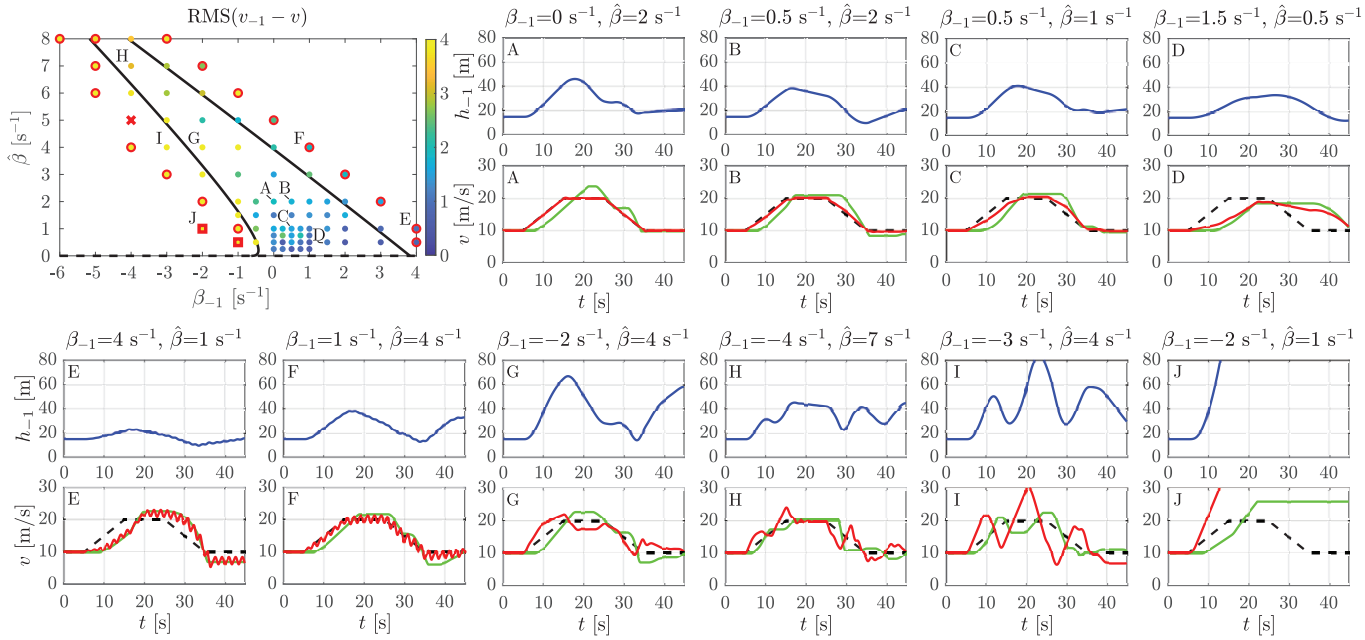

Fig. 4. Stability chart for subject #1 in the plane of the control gains of the AV and time signals of ten particular measurements. In the stability chart, the solid and dashed black lines show the theoretical dynamic and static stability boundaries corresponding to the estimated parameters of subject #1 (see Table I). The measurement points are colored according to the RMS of the velocity difference ($v_{-1} - v$). In the small panels, the blue curves refer to the headway, the black-dashed curve is the reference velocity, while the green and red curves correspond to the velocity profile of the HV and the AV, respectively.

IV. Results of HITL Tests

Nine human drivers participated in the experiments; two female and seven male subjects, all in the age group 24–30. Each of them performed the driving task for 79 control gain combinations of the AV. These combinations cover the theoretical stability boundary, such that there are more points within the relevant region of small control gains than close to the calculated stability boundaries. The experiments were carried out according to the principles of the Declaration of Helsinki, and the subjects were allowed to withdraw from the research at any time.

Fig. 4 presents the stability chart corresponding to the measurement of subject #1, while the small panels show the time signals in the case of ten particularly selected control gain combinations of the AV. In the stability chart, the measurement points are colored according to the root mean square (RMS) of the velocity difference ($v_{-1} - v$). Red circles refer to control gain combinations at which the AV performed saturated braking, while red squares denote measurements when the AV accelerated above 50 m/s. Finally, the red cross indicates that the vehicles collided during the corresponding driving tasks. In the small panels, the red and green curves refer to the velocities of the AV and HV, respectively, while the reference

velocity is denoted with black dashed line. Furthermore, the blue curves in the separate panels present the time evolution of the headway h_{-1} during the measurements.

In the case of AV gain combination A, the backward looking control gain is set at $\beta_{-1} = 0$ s^{-1}, that is, the AV is traveling with a simple cruise control and it does not respond to the velocity of the HV. In this case, the AV follows accurately the reference, while the velocity of the HV has a slight overshoot.

At the points B-D, the control gain ratio $\beta_{-1}/\hat{\beta}$ increases, that is, the AV takes into account the velocity of the HV with increasing weight, which yields larger and larger deviations compared to the reference. First, this phenomenon helps the human operator as the velocity profile of the AV becomes smoother; however, excessively large deviations from the reference should also be avoided.

Gain combinations E and F are already outside of the theoretical dynamic stability boundary, which is in accordance with the oscillations in the velocity profile of the AV. During the oscillations, the acceleration and deceleration of the AV saturates, therefore, the amplitudes of the oscillations do not increase. Furthermore, again, the ratio of the control gains determines whether the velocity of the AV oscillates around the velocity of the HV or around the reference velocity. Note that the human operator does not respond to these high-frequency oscillations. The corresponding theoretical model, discussed in [24], predicts that the angular frequency of the oscillations is $\Omega_{\mathrm{AV,pred}} \approxeq \pi/(2\sigma)$. This corresponds to a time period of $T_{\mathrm{pred}} \approxeq 1.6$ s (that is, $f_{\mathrm{pred}} \approxeq 0.6$ Hz), which is in accordance with the measurement results.

In the combinations discussed so far, β_{-1} was positive yielding that the AV kept its velocity between the reference velocity and the velocity of the HV. In contrast, if $\beta_{-1} < 0$, then the AV accelerates more aggressively than the reference signal, which can be considered as if the AV tried to "pull" the HV. However, in case of deceleration, the AV is braking harder than it should, which yields situations as if the AV performed a "brake checking" in front of the HV. Close to the stability boundaries, this phenomenon sometimes leads to collisions.

Point G is still within the stable domain, however, both the velocities of the AV and the HV present significant deviations from the reference. Combination H is close to the theoretical double Hopf bifurcation point, which can be observed in the measurement results as well. A low-frequency $f_{\mathrm{low}} \approx 0.14$ Hz oscillation with large amplitude dominates the velocity profile of the AV, however, around $t = 20$ s and after $t = 35$ s, one can observe a high-frequency small-amplitude oscillation of $f_{\mathrm{high}} \approx 0.6$ Hz as well.

Finally, points I and J yield strongly undesirable control gain combinations. In the first case, the AV performs extremely large amplitude oscillations, while in the second case, it accelerates continuously without braking.

All in all, the human operator filters out the high-frequency oscillations of the AV and sometimes applies a kind of act and wait control [30]. Moreover, the human driving behavior is not deterministic: facing twice the same situation yields only similar but somewhat different responses. Still, the theoretical stability boundary matches well with the experiments. This motivated us to fit the parameters of the theoretical model to the measurement results.

The identification of the parameters in a delay-free system has a broad literature [31], [32], [33]. However, the simultaneous estimation of the feedback gains and the delay is still a challenging task [34], [35], [36], [37]. For the estimation of the human control parameters, we apply the method of sweeping least squares [20], which allows to fit the control gains and the corresponding time delay, while the high-frequency disturbances are filtered out.

Let us denote the kth sampling instance by $t_k = k\Delta t$, at which the state variables are

$$\hat{h}_{-1}[k] = h_{-1}(t_k) - h_{\mathrm{stop}}, \quad v_{-1}[k] = v_{-1}(t_k), \ v[k] = v(t_k). \tag{16}$$

Here, the headway is shifted with the h_{stop} value, which allows to obtain a linear right-hand side in (2). Using the explicit Euler method, the discretization of (2) yields

$$\frac{v[k+1] - v[k]}{\Delta t} = \alpha\left(\kappa\hat{h}_{-1}[k-m] - v_{-1}[k-m]\right) + \beta\left(v[k-m] - v_{-1}[k-m]\right) \tag{17}$$

where $m = \mathrm{round}(\tau/\Delta t)$ is the still unknown discrete delay.

Let us introduce the new variables

$$a = -\alpha - \beta, \quad b = \alpha\kappa, \ c = \beta \tag{18}$$

which form the unknown coefficients of the state variables v_{-1}, h_{-1}, and v, respectively. Assume that the driver reaction time is within the interval $\tau \in [\tau_{\min}, \tau_{\max}]$ and discretize it with the discrete delay $m \in \{m_{\min}, \dots, m_{\max}\}$, where $\tau_{\min} = m_{\min}\Delta t$ and $\tau_{\max} = m_{\max}\Delta t$. Then, considering $N+1$ data points over the time window $N\Delta t$, the gains corresponding to any discrete delay m can be estimated as

$$\begin{bmatrix} a_{\mathrm{est}}(m) \\ b_{\mathrm{est}}(m) \\ c_{\mathrm{est}}(m) \end{bmatrix} = \left(\mathbf{P}^{\mathsf{T}}(m)\mathbf{P}(m)\right)^{-1}\mathbf{P}^{\mathsf{T}}(m)\mathbf{Q} \tag{19}$$

where

$$\mathbf{P}(m) = \begin{bmatrix} v_{-1}[k-m] & \hat{h}_{-1}[k-m] & v[k-m] \\ \vdots & \vdots & \vdots \\ v_{-1}[k+N-m] & \hat{h}_{-1}[k+N-m] & v[k+N-m] \end{bmatrix} \tag{20}$$

and

$$\mathbf{Q} = \frac{1}{\Delta t}\begin{bmatrix} v_{-1}[k+1] - v_{-1}[k] \\ \vdots \\ v_{-1}[k+N+1] - v_{-1}[k+N] \end{bmatrix}. \tag{21}$$

Note that the data size N should be larger than the maximum discrete delay $m_{\max}$.

We want to minimize the corresponding fitting error

$$R(m) = \left\| \mathbf{P}(m)\begin{bmatrix} a_{\mathrm{est}}(m) \\ b_{\mathrm{est}}(m) \\ c_{\mathrm{est}}(m) \end{bmatrix} - \mathbf{Q} \right\| \tag{22}$$

over the range of the potential discrete delays. Therefore, the time delay is estimated as $\tau_{\mathrm{est}} = m_{\mathrm{est}}\Delta t$, where

$$m_{\mathrm{est}} = \arg\min_{m} R(m) \tag{23}$$

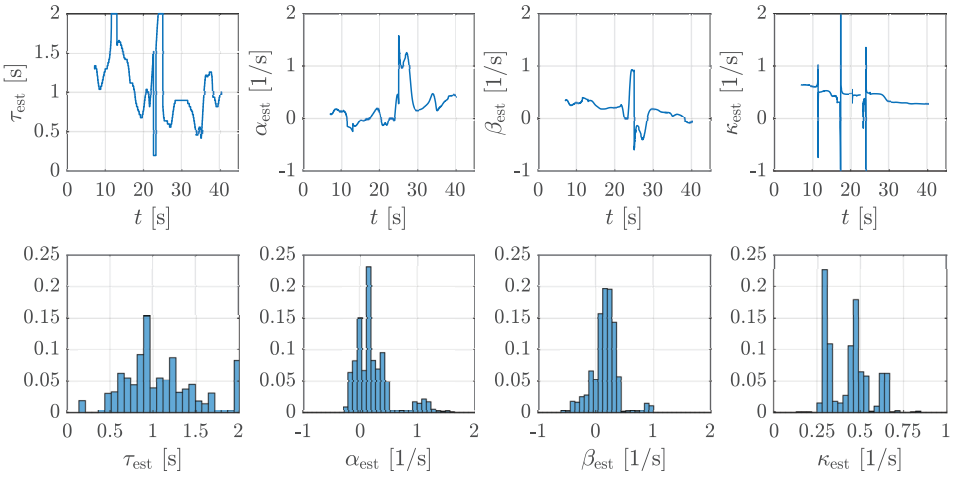

Fig. 5. Parameters estimated with the help of the sweeping least squares method corresponding to point H in Fig. 4.

TABLE I
AVERAGE OF THE ESTIMATED PARAMETERS FOR EACH SUBJECT

	τ [s]	α [1/s]	β [1/s]	κ [1/s]
S1	1.04	0.23	0.16	0.53
S2	0.76	0.22	0.60	0.77
S3	0.83	0.30	0.28	0.50
S4	0.68	0.24	0.38	1.04
S5	0.95	0.23	0.27	0.63
S6	0.83	0.20	0.23	0.66
S7	0.84	0.38	0.25	0.50
S8	0.88	0.25	0.24	0.57
S9	0.80	0.27	0.20	0.45
Mean	0.85	0.26	0.29	0.63

while the estimated control gains are

$$\alpha_{est} = -a_{est}(m_{est}) - c_{est}(m_{est})$$
$$\beta_{est} = c_{est}(m_{est}), \quad \kappa_{est} = \frac{b_{est}(m_{est})}{\alpha_{est}}. \tag{24}$$

The above described algorithm was carried out at every time steps $k > m_{max}$. During the evaluation of the measurements, the time delay was varied between $\tau_{min} = 0.2$ s and $\tau_{max} = 2$ s. Therefore, the discrete delay was selected from the set $m \in \{10, 12, \ldots, 100\}$ with $\Delta t = 0.02$ s. We considered $h_{stop} = 0$ m as in [20] as well, although, this parameter may be important in case of other traffic situations, for example, if the leading vehicle stops. Finally, we used $N = 500$ corresponding to the window size 10 s.

Fig. 5 presents the results of the sweeping least squares method corresponding to point H of Fig. 4. The panels in the first row show the variation of the estimated values in time. The value calculated in each time window is displayed at the time corresponding to the center of the window. The panels in the second row present the distributions of the parameters in normalized histograms. The time delay varies around $\tau_{est} = 1$ s, while it takes larger values during the first half and smaller values during the second half of the measurement. This reflects that the operator reacts faster during the deceleration period (that may result in more dangerous situations) than during the acceleration period. The control gains α_{est} and β_{est} vary around 0.2 s^{-1}, while the mean value of κ_{est} is somewhat higher. Since the calculation of κ_{est} involves a division, it contains a few singular data points but the vast majority of the points are located between 0.25 and 0.75 s^{-1}.

Note that the histogram of the time delay takes relatively large values at the boundaries, which does not fit to the distribution of the central part. The large column at $\tau_{est} = \tau_{max} = 2$ s appears because of the "safety-critical filter" of the human operator, that is, the operator did not aim to follow immediately the acceleration of the AV or did not respond immediately to the brake lights if the headway was large enough. In contrast, the reaction time was small in case of the safety-critical situations.

The column at $\tau_{est} = \tau_{min} = 0.2$ s indicates some questionable data; the reaction time of the human operators—together with the computer delay—cannot be as small as that. In [38], the human reaction time was measured in a HITL environment via two methods: an instant reaction test and a blank-out test. With both methods, the reaction times were larger than 0.2 s. Additionally, in these tests, the reaction times were measured through the hands, while in the direction of the legs, it must be even larger [39]. Clearly, the imperfection of the method of sweeping least squares applied for the given limited amount of data resulted in the tiny unrealistic column in the identified delay distribution. Thus, the data points corresponding to $\tau_{est} = \tau_{max}$ and $\tau_{est} = \tau_{min}$ and the corresponding α_{est}, β_{est}, and κ_{est} values are not taken into account during the following calculations.

All the nine human subjects performed the driving task for the 79 control gain combinations of the AV and the sweeping least squares method was applied for the data of each measurement. Then, we determined the mean estimated values for each subject examining the data obtained from the 79 points together, which is summarized in Table I.

The estimated values are in the same range as it was obtained in [20] based on experiments with real cars. There is an interesting statement in [40] that a chain of HVs cannot be string stable if the reaction time is larger than $\tau_{cr} = 1/(2\kappa)$. Here, subject #1 is at the border of this critical value. However, the presence of the automated vehicle with appropriately

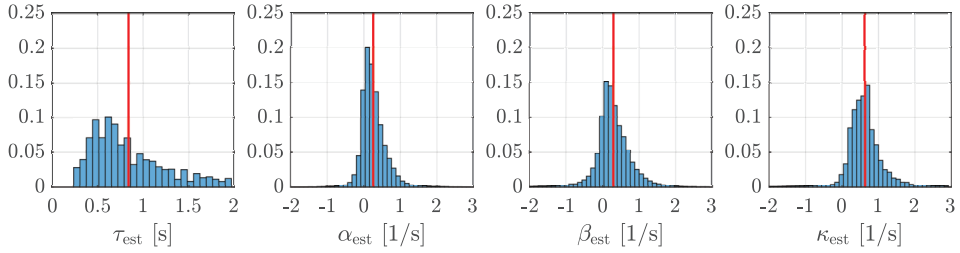

Fig. 6. Histograms of the estimated parameters taking into account all the measurements.

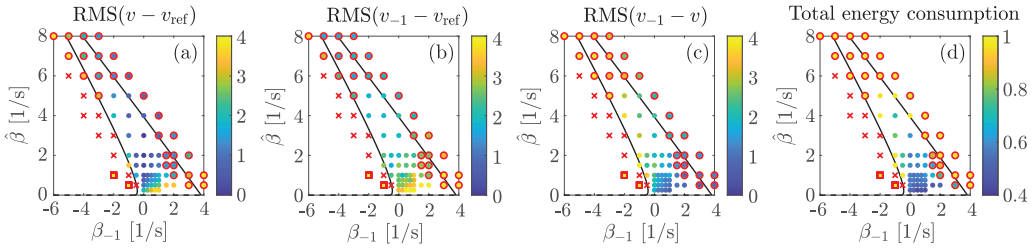

Fig. 7. Comparison of the measurement results and the theoretical stability chart determined for the mean value of the estimated parameters of the nine subjects (see Table I). The dashed and solid black lines present the static and dynamic stability boundaries, respectively. The measurement points are colored according to the mean values of the nine subjects; the colorbars refer to the RMS of the relative velocities (a) $(v - v_{\text{ref}})$, (b) $(v_{-1} - v_{\text{ref}})$, (c) $(v_{-1} - v)$, while in panel (d) coloring reflects the total energy consumption.

tuned control gains can extend this boundary as it could be predicted from the study [24], where the same car-following configuration was analyzed.

Furthermore, Fig. 6 shows the normalized histograms which include all the measurements of all the nine subjects; with the red vertical lines indicating the mean values of the corresponding parameters. The parameters α_{est}, β_{est}, and κ_{est} have sharp peaks close to the mean values. In contrast, although the time delay distribution also has a peak at around 0.6 s, it is less dominant, and the distribution is not symmetric but elongated to the right. This phenomenon is known in the literature [41]; it is often approximated by gamma distribution and related to the safety-critical response of the drivers discussed above.

Finally, the measurement points in Fig. 7(a)–(c) are colored according to the RMS of the relative velocities $(v - v_{\text{ref}})$, $(v_{-1} - v_{\text{ref}})$, and $(v_{-1} - v)$, while in panel (d), the coloring reflects the total energy consumption normalized by the weights of the vehicles and by the distance traveled [8]

$$w_i(t) = \frac{\int_0^t v_i(\theta) g\left(\dot{v}_i(\theta)\right) \mathrm{d}\theta}{\int_0^t v_i(\theta) \mathrm{d}\theta}. \tag{25}$$

Here, we assume that braking does not require and does not regenerate energy:

$$g(\dot{v}_i) = \max\{0, \dot{v}_i\}. \tag{26}$$

Red crosses indicate the control gain combinations, at which at least one collision occurred, red circles denote the points, at which the AV performed saturated braking in case of at least two subjects, while red squares refer to combinations at which the AV accelerated above 50 m/s. These critical control gain combinations match well with the solid black curve of the theoretical dynamic stability boundary that is obtained by means of the mean estimated values of the human parameters (see Table I).

In accordance with the expectations, the AV follows the reference speed best when the backward looking gain is zero, that is, the AV is not influenced by the HV. If β_{-1} dominates over $\hat{\beta}$, the velocity of both vehicles deviate significantly from the reference, which is in accordance with the proximity of the static stability boundary at $\hat{\beta} = 0$ [1/s]. In contrast, panel (c) shows that positive values of the gain β_{-1} help the human operator to smoothly follow the lead vehicle. Finally, the large values of the total energy consumption also cover well the theoretical dynamic stability boundary, since the AV starts to oscillate close to the boundary which significantly increases the energy consumption.

V. Conclusion

The simplest scenario of mixed traffic was investigated where an automated vehicle guided the motion of a HV. A mathematical model was introduced to represent the human behaviors and controller was proposed for the AV to respond to a reference velocity and to the motion of the HV simultaneously. The model was validated using HITL experiments where the human control parameters were carefully identified.

The experimental results imply that the theoretical stability boundaries provide not only qualitatively but also quantitatively appropriate restriction of the domain from where the control gains of the AV should be selected. However, according to the HITL experiments, the negative values of the backward looking gain should be avoided. Furthermore, during the tuning of the control gains of the AV, one should balance between the smooth guidance of the human driver and the accurate following of the reference velocity. Although this balance is a difficult choice and the resulting performance will vary from driver to driver, the control gain combination $\beta_{-1} \approx 0.5$ [1/s] and $\hat{\beta} \approx 0.5$ [1/s] seems to be a reasonable compromise.

In the future, we plan to explore further methods for the estimation of the human parameters, which may lead to improved results. For example, neural networks [36], [42] and the Bayesian inference-based algorithms [35] have been applied to problems where the time delay is a critical unknown

parameter. In addition, the string stability of vehicle platoons is also an important concern [15], [24]; it should be investigated in field tests.

After the extensive HITL tests, experiments with real vehicles in real environment should start when the human driver also feels the variation in the reaction forces caused by the vehicle's acceleration/deceleration. This study provides a good basis for that, since during real car experiments, one can focus on the relevant domain of control gains only.

REFERENCES

[1] D. Caveney, "Cooperative vehicular safety applications," *IEEE Control Syst. Mag.*, vol. 30, no. 4, pp. 38–53, Aug. 2010.

[2] G. Orosz, "Connected cruise control: Modelling, delay effects, and nonlinear behaviour," *Vehicle Syst. Dyn.*, vol. 54, no. 8, pp. 1147–1176, Aug. 2016.

[3] L. Zhang and G. Orosz, "Motif-based design for connected vehicle systems in presence of heterogeneous connectivity structures and time delays," *IEEE Trans. Intell. Transp. Syst.*, vol. 17, no. 6, pp. 1638–1651, Jun. 2016.

[4] S. S. Avedisov and G. Orosz, "Analysis of connected vehicle networks using network-based perturbation techniques," *Nonlinear Dyn.*, vol. 89, no. 3, pp. 1651–1672, Aug. 2017.

[5] S. Li, L. Yang, and Z. Gao, "Coordinated cruise control for high-speed train movements based on a multi-agent model," *Transp. Res. C, Emerg. Technol.*, vol. 56, pp. 281–292, Jul. 2015.

[6] S. E. Li, Q. Guo, L. Xin, B. Cheng, and K. Li, "Fuel-saving servo-loop control for an adaptive cruise control system of road vehicles with step-gear transmission," *IEEE Trans. Veh. Technol.*, vol. 66, no. 3, pp. 2033–2043, Mar. 2017.

[7] J. Lioris, R. Pedarsani, F. Y. Tascikaraoglu, and P. Varaiya, "Platoons of connected vehicles can double throughput in urban roads," *Transp. Res. C, Emerg. Technol.*, vol. 77, pp. 292–305, Apr. 2017.

[8] T. G. Molnár, M. Hopka, D. Upadhyay, M. Van Nieuwstadt, and G. Orosz, "Virtual rings on highways: Traffic control by connected automated vehicles," in *AI-Enabled Technologies for Autonomous and Connected Vehicles*. Cham, Switzerland: Springer, 2023, pp. 441–479.

[9] J. Vander Werf, S. E. Shladover, M. A. Miller, and N. Kourjanskaia, "Effects of adaptive cruise control systems on highway traffic flow capacity," *Transp. Res. Rec., J. Transp. Res. Board*, vol. 1800, no. 1, pp. 78–84, Jan. 2002.

[10] B. van Arem, C. J. G. van Driel, and R. Visser, "The impact of cooperative adaptive cruise control on traffic-flow characteristics," *IEEE Trans. Intell. Transp. Syst.*, vol. 7, no. 4, pp. 429–436, Dec. 2006.

[11] S. E. Shladover, D. Su, and X.-Y. Lu, "Impacts of cooperative adaptive cruise control on freeway traffic flow," *Transp. Res. Rec.*, vol. 2324, no. 1, pp. 63–70, 2012.

[12] S. E. Shladover, C. Nowakowski, X.-Y. Lu, and R. Ferlis, "Cooperative adaptive cruise control: Definitions and operating concepts," *Transp. Res. Rec.*, vol. 2489, no. 1, pp. 145–152, Jan. 2015.

[13] J. I. Ge, S. S. Avedisov, C. R. He, W. B. Qin, M. Sadeghpour, and G. Orosz, "Experimental validation of connected automated vehicle design among human-driven vehicles," *Transp. Res. C, Emerg. Technol.*, vol. 91, pp. 335–352, Jun. 2018.

[14] W. B. Qin, M. M. Gomez, and G. Orosz, "Stability and frequency response under stochastic communication delays with applications to connected cruise control design," *IEEE Trans. Intell. Transp. Syst.*, vol. 18, no. 2, pp. 388–403, Feb. 2016.

[15] J. Wang, Y. Zheng, C. Chen, Q. Xu, and K. Li, "Leading cruise control in mixed traffic flow: System modeling, controllability, and string stability," *IEEE Trans. Intell. Transp. Syst.*, vol. 23, no. 8, pp. 12861–12876, Aug. 2021.

[16] Q. Wang et al., "Adaptive leading cruise control in mixed traffic considering human behavioral diversity," *IEEE Trans. Intell. Transp. Syst.*, vol. 25, no. 6, pp. 5059–5070, Jun. 2024.

[17] C. Zhao, H. Yu, and T. G. Molnar, "Safety-critical traffic control by connected automated vehicles," *Transp. Res. C, Emerg. Technol.*, vol. 154, Sep. 2023, Art. no. 104230.

[18] J. Zhao, Y. Chen, and Y. Gong, "Study of connectivity probability of vehicle-to-vehicle and vehicle-to-infrastructure communication systems," in *Proc. IEEE 83rd Veh. Technol. Conf. (VTC Spring)*, May 2016, pp. 1–4.

[19] C. R. Storck and F. Duarte-Figueiredo, "A survey of 5G technology evolution, standards, and infrastructure associated with vehicle-to-everything communications by Internet of Vehicles," *IEEE Access*, vol. 8, pp. 117593–117614, 2020.

[20] J. I. Ge and G. Orosz, "Connected cruise control among human-driven vehicles: Experiment-based parameter estimation and optimal control design," *Transp. Res. C, Emerg. Technol.*, vol. 95, pp. 445–459, Oct. 2018.

[21] D. Lee, S. Lee, Z. Chen, B. B. Park, and D. H. Shim, "Design and field evaluation of cooperative adaptive cruise control with unconnected vehicle in the loop," *Transp. Res. C, Emerg. Technol.*, vol. 132, Nov. 2021, Art. no. 103364.

[22] B. A. Guvenc and E. Kural, "Adaptive cruise control simulator: A low-cost, multiple-driver-in-the-loop simulator," *IEEE Control Syst. Mag.*, vol. 26, no. 3, pp. 42–55, Jun. 2006.

[23] G. Mastinu, D. Biggio, F. Della Rossa, and M. Fainello, "Straight running stability of automobiles: Experiments with a driving simulator," *Nonlinear Dyn.*, vol. 99, no. 4, pp. 2801–2818, Mar. 2020.

[24] B. Szaksz, G. Orosz, and G. Stépán, "Guided control of a human driver via an automated vehicle," *IFAC-PapersOnLine*, vol. 56, no. 2, pp. 899–904, 2023.

[25] B. Szaksz, G. Orosz, and G. Stépán, "Nonlinear guidance of a human driver via an automated vehicle," in *Proc. IUTAM Symp. Nonlinear Dyn. Design Mech. Syst. Across Different Length/Time Scales*. Cham, Switzerland: Springer, 2025, pp. 405–416.

[26] M. A. Hossain, K. A. Kabir, and J. Tanimoto, "Improved car-following model considering modified backward optimal velocity and velocity difference with backward-looking effect," *J. Appl. Math. Phys.*, vol. 9, no. 2, pp. 242–259, 2021.

[27] M. Bando, K. Hasebe, K. Nakanishi, and A. Nakayama, "Analysis of optimal velocity model with explicit delay," *Phys. Rev. E, Stat. Phys. Plasmas Fluids Relat. Interdiscip. Top.*, vol. 58, no. 5, p. 5429, 1998.

[28] T. Insperger and G. Stepan, *Semi-Discretization for Time-Delay Systems: Stability and Engineering Applications*, vol. 178. New York, NY, USA:Springer 2011.

[29] (2024). *Esperanza High Octane Steering Wheel*. [Online]. Available: https://esperanza.pl/szczegolyProduktu.php?kat=231&item=760&lan=4&cur=2

[30] G. Stepan and T. Insperger, "Stability of time-periodic and delayed systems—A route to act-and-wait control," *Annu. Rev. Control*, vol. 30, no. 2, pp. 159–168, 2006.

[31] O. Nelles, *Nonlinear System Identification*. Cham, Switzerland: Springer, 2020, pp. 831–891.

[32] H. Chen, H. Liu, X. Chu, Q. Liu, and D. Xue, "Anomaly detection and critical SCADA parameters identification for wind turbines based on LSTM-AE neural network," *Renew. Energy*, vol. 172, pp. 829–840, Jul. 2021.

[33] Y. Xue, Y. Liu, C. Ji, G. Xue, and S. Huang, "System identification of ship dynamic model based on Gaussian process regression with input noise," *Ocean Eng.*, vol. 216, Nov. 2020, Art. no. 107862.

[34] J. Na, X. Ren, and Y. Xia, "Adaptive parameter identification of linear SISO systems with unknown time-delay," *Syst. Control Lett.*, vol. 66, pp. 43–50, Apr. 2014.

[35] X. A. Ji, T. G. Molnár, A. A. Gorodetsky, and G. Orosz, "Bayesian inference for time delay systems with application to connected automated vehicles," in *Proc. IEEE Int. Intell. Transp. Syst. Conf. (ITSC)*, Sep. 2021, pp. 3259–3264.

[36] X. A. Ji and G. Orosz, "Trainable delays in time delay neural networks for learning delayed dynamics," *IEEE Trans. Neural Netw. Learn. Syst.*, vol. 36, no. 3, pp. 5219–5229, Mar. 2025.

[37] T. Zhang, Z. Lu, J. Liu, and G. Liu, "Parameter identification of nonlinear systems with time-delay from time-domain data," *Nonlinear Dyn.*, vol. 104, pp. 4045–4061, Apr. 2021.

[38] B. A. Kovacs and T. Insperger, "Virtual stick balancing: Skill development in Newtonian and aristotelian dynamics," *J. Roy. Soc. Interface*, vol. 19, no. 188, Mar. 2022, Art. no. 20210854.

[39] B. D. Greenshields, "Reaction time in automobile driving," *J. Appl. Psychol.*, vol. 20, no. 3, pp. 353–358, 1936.

[40] G. Orosz and T. Molnar, *Dynamics and Control of Connected Vehicles*. Cham, Switzerland: Springer, 2025.

[41] R. Ratcliff, "Group reaction time distributions and an analysis of distribution statistics," *Psychol. Bull.*, vol. 86, no. 3, p. 446, 1979.

[42] X. A. Ji, T. G. Molnár, S. S. Avedisov, and G. Orosz, "Feed-forward neural networks with trainable delay," in *Proc. 2nd Conf. Learn. Dyn. Control*, vol. 120, 2020, pp. 127–136.